Oriented Microstructures of Polystyrene-*b*-poly(L-lactide) Thin Films Induced by Crystallizable Solvents

Wen-Hsien Tseng,[†] Ping-Yen Hsieh,[‡] Rong-Ming Ho,*[,†] Bor-Han Huang,[§] Chu-Chien Lin,[§] and Bernard Lotz[⊥]

Department of Chemical Engineering, National Tsing-Hua University, Hsinchu 30013, Taiwan, Department of Chemical Engineering, National Chung-Hsing University, Taichung 40227, Taiwan, Department of Chemistry, National Chung-Hsing University, Taichung 40227, Taiwan, and Institut Charles Sadron (CNRS−ULP), 6, rue Boussingault, 67083 Strasbourg, France

Received April 21, 2006; Revised Manuscript Received June 28, 2006

ABSTRACT: Polystyrene-*b*-poly(L-lactide) (PS−PLLA) diblock copolymers with high and low molecular weights were synthesized to form strongly and weakly segregated thin-film morphologies, respectively (i.e., ordered lamellar and disordered textures). Large-sized, well-oriented lamellar microstructures of PS−PLLA thin films were produced for both samples by using the crystallizable solvents: benzoic acid (BA) and hexamethylbenzene (HMB). In strongly segregated (high M_n) PS−PLLA, the oriented microstructures were obtained through the PS−PLLA microphase separation due to directional crystallization of crystallizable solvents at the eutectic point (*directional eutectic solidification*) regardless of the PLLA crystallization. Lattice matching between crystalline substrates and PLLA was found to be nonessential for inducing microstructure orientation although it may improve its orientation order. In weakly segregated (low M_n) PS−PLLA, the oriented microstructures were formed through the directional crystallization of PLLA on the substrates (*crystallization-induced orientation*) regardless of the directional eutectic solidification and lattice matching. Two mechanisms: of directional eutectic solidification and of crystallization-induced oriented microstructure have thus been identified. Oriented, defined lamellar trenches can be prepared by hydrolysis of PLLA component, providing a possible path to prepare nanopatterned templates with lamellar nanochannels.

Introduction

Nanopatterning, the creation of patterns with nanoscale features, has drawn great attention in recent years due to its promising applications in nanotechnologies. Large-sized, well-oriented periodic arrays would be needed for practical applications. A variety of new patterning technologies (including top-down and bottom-up methods, in particular, nanopatterning from the self-assembly of block copolymers) have been developed, which try to create well-defined nanopatterns over large areas.[1] Different approaches to control the orientation of microphase-separated microstructures in block copolymers have been used: solution casting,[2−10] shear fields,[11−15] electric fields,[16,17] surface effect,[18−20] patterned substrates,[21−23] temperature gradients,[24] graphoepitaxy,[25,26] and crystallizable solvents.[27−31] Strategies for the orientation control of microphase-separated microdomains depend strongly upon the intrinsic microstructures of block copolymers and the sample thickness. Oriented cylindrical microdomains in large area were induced by shear fields[14] in bulk (thickness > 100 nm) and by solution casting[2,4,5,8,10] and electric fields[15,16] in the thin-film samples (thickness < 100 nm). By contrast, the orientation of lamellar microdomains can be achieved in bulk by methods such as shear fields and temperature gradients. Different oriented textures, with the lamellar normal vertical, parallel, and transverse to the substrate, respectively, have been obtained in bulk by adjusting strain and frequency during shearing.[14] Parallel orientation could be obtained by roller casting,[15] temperature gradients[24] and rimming coating.[32] For lamellar thin-film samples, parallel lamellar orientation can be formed by preferential substrates whereas perpendicular orientation can be created by using neutral substrates but lack long-range lateral orientation order.[18,19]

Recently, an easy way to create large-sized, well-oriented cylindrical and lamellar microdomains of semicrystalline block copolymers in thin films has been proposed by De Rosa and co-workers.[27−29] The induced microstructure orientation of strongly segregated block copolymers is described in full as directional eutectic solidification, the directional solidification of microphase separation induced by directional crystallization of crystallizable solvents at eutectic point. The aspects of the directional eutectic solidification can be realized by dividing the process into three stages using a hypothetical solvent−polymer phase diagram (Figure 3 in ref 27). An important feature of the phase diagram is the presence of a eutectic due to the intersection of the melting-point depression liquidus curve of the crystallizable solvent with the microphase-separation-transition depression liquidus curve of the block copolymer. First, the block copolymer and the crystallizable solvent form a homogeneous liquid above the melting temperature of the crystallizable solvent. Second, when the temperature is dropped below the melting-point depression liquidus curve of the crystallizable solvent, the directional crystallization growth of crystallizable solvent is initiated by which increases the copolymer content of the remaining liquid toward the eutectic liquid. Further cooling to the eutectic temperature, the eutectic liquid is eventually directionally solidified by thickening the preexisting crystalline substrate and transforms into crystalline substrate and an ordered, microphase-separated block copolymer (*directional eutectic solidification*). This mechanism differs from

* To whom correspondence should be addressed. Telephone: 886-3-5738349. Fax: 886-3-5715408. E-mail: rmho@mx.nthu.edu.tw.
[†] Department of Chemical Engineering, National Tsing-Hua University.
[‡] Department of Chemical Engineering, National Chung-Hsing University.
[§] Department of Chemistry, National Chung-Hsing University.
[⊥] Institut Charles Sadron (CNRS−ULP).

10.1021/ma0608929 CCC: $33.50
Published on Web 09/07/2006

epitaxial crystallization that induces specific molecular chain orientation due to lattice matching.[27,28,31,33−35] In our previous studies,[30] large-sized, well-oriented lamellar microstructure of weakly segregated poly(L-lactide)-*b*-poly(ϵ-caprolactone) (PLLA−PCL) thin films were also obtained by using different crystalline substrates (benzoic acid (BA) and hexamethylbenzene (HMB)) whereas disordered textures are formed on amorphous substrates due to the weak segregation strength in the studied temperature range.[30] We hypothesize that the lamellar microstructure orientation in weakly segregated block copolymers is mainly due to directional crystallization of PLLA on the crystalline substrates (*crystallization-induced orientation*) rather than directional eutectic solidification. In fact, the microstructure orientation of crystalline block copolymers is the consequence of both block copolymer microphase separation and crystallization of the crystallizable block interacting with the crystalline substrate.

The objective of this study is to clarify the origins of the induced microstructure orientation and better differentiate the mechanisms of directional eutectic solidification and crystallization-induced orientation. Weakly and strongly segregated samples of polystyrene-*b*-poly(L-lactide) (PS−PLLA) diblock copolymers with different molecular weights were used. PS−PLLAs in the presence of crystallizable solvent were isothermally treated and quenched (see Experimental section for details). Crystallizable solvents including BA and HMB (that is crystalline substrates with and without lattice matching to crystalline PLLA, respectively) were used to examine the role of lattice matching in microstructure orientation.

Block copolymers such as PS−PLLA are a new family for the preparation of nanopatterned templates because polyester blocks (i.e., PLLA) can be selectively degraded by hydrolysis treatment.[36−38] Recently, ordered cylindrical nanoporous polymers from poly(styrene)-*b*-poly(D,L-lactide) (PS−PLA) block copolymers was produced in bulk by simple chemical etching of PLA.[37] In contrast, we produced cylindrical nanoporous thin films from spin-coated PS−PLLA.[10] In this study, large-sized, well-oriented lamellar microstructures of PS−PLLA are formed with the help of crystalline substrates. Selective degradation of the PLLA component yields nanopatterned templates with lamellar nanochannels or trenches.

Experimental Section

Materials. A two-step polymerization was used to synthesize the PS−PLLA copolymer. A hydroxyl-terminated polystyrene was formed by free radical polymerization of styrene by using 4-hydroxy-2,2,6,6-tetramethylpiperidine-*N*-oxyl, 4-hydroxy-TEMPO (4-OH-TEMPO), as initiator in the presence of dibenzoylperoxide (BPO). The PS-TEMPO-4-OH was further reacted with $[(\mu_3\text{-EDBP})Li_2]_2[(\mu_3\text{-}^n\text{Bu})Li(0.5Et_2O)]_2$, giving a macroinitiator. The $[(\mu_3\text{-EDBP})Li_2]_2$ $[(\mu_3\text{-}^n\text{Bu})Li(0.5Et_2O)]_2$ was prepared according to the method described previously.[39] PS−PLLA was then prepared by the control led ring-opening polymerization of L-lactide in the presence of the macroinitiator. The detailed synthetic routes and conditions were reported in our previous paper.[40]

Gel permeation chromatography (GPC) measurements were performed on a Hitachi L-7100 system equipped with a differential Bischoff 8120 RI detector using THF (HPLC grade) as an eluent. Molecular weight and molecular weight distributions were calculated using polystyrene as standard. The number-average molecular weight (M_n) of 4-hydrolysis-TEMPO terminated PS and polydispersity (PDI) of PS−PLLA block copolymer were measured by GPC. The molecular weights of PLLA blocks and PS−PLLA block copolymers were measured by ^{1}H NMR. The volume fraction of PLLA was calculated by assuming densities of PS and PLLA to be 1.02 and 1.248 g/cm^3. The details of samples are listed in Table 1.

Table 1. Characteristic of the PS−PLLA Block Copolymers

entry	$M_{n,PS}$ [g/mol][a]	$M_{n,PLLA}$ [g/mol][b]	PDI[c]	f_{PS}[v]
S03-L05	3800	4650	1.20	0.51
S14-L15	13 600	15 300	1.16	0.52

[a] Measured from GPC analysis. [b] Obtained from integration of ^{1}H NMR measurement. [c] Measured from GPC analysis.

Sample Preparation. Two major procedures were used to investigate the mechanisms of induced orientation in the PS−PLLA thin-film microstructures: isothermal crystallization and quenching. For isothermally treated samples, the procedure described by De Rosa and co-workers was followed.[27] PS−PLLA films were first formed on carbon-coated microscope glass slides by spin-coating from chlorobenzene (C_6H_5Cl) solution (1.5 wt % of PS−PLLA) at room temperature. The film thickness was ca. 50 nm, as determined by scanning probe microscopy (SPM). The crystallizable solvents in powder form were spread on a glass coverslip. The glass slide with polymer-side down was placed on the glass coverslip. The assembly was heated and the polymer dissolved at 150 and 170 °C in the presence of BA (T_m = 123 °C) and HMB (T_m = 168 °C), respectively. The assembly was cooled at 80 °C on a hot plate. Crystallization of the solvents produced large, elongated crystals with the *b* axis parallel to the growth-front, with concomitant crystallization of the PS−PLLA. After cooling to room temperature, the glass slide and coverslip were separated, and the crystalline substrates were dissolved in ethyl alcohol at 50 °C (BA) and in acetone at room temperature (HMB). Quenching was used to avoid PLLA crystallization. The procedure was as above, but the assembly of sandwiched thin films was quenched in the liquid nitrogen, instead isothermally annealed at a hot plate. In all cases, the composite polymer−carbon film was floated onto water and picked on TEM copper grids.

Differential Scanning Calorimetry (DSC). Perkin-Elmer DSC 7 instrument was used for the DSC investigation. The S03L05 and S14L15 samples have melting temperature of 152 and 149 °C, respectively. The maximum crystallization temperatures of S03L05 and S14L15 under 10 °C/min cooling rate are 110 and 82 °C, respectively. T_g of PLLA and PS for S03L05 are 52 and 81 °C, respectively, whereas T_g of PLLA and PS for S14L15 are 50 and 92 °C, respectively.

Transmission Electron Microscopy (TEM). Bright field TEM images and selected area electron diffraction (SAED) were performed with a JEOL TEM-1200x transmission electron microscopy, at an accelerating voltage of 120 kV. The PS−PLLA thin films were stained by exposure to the vapors of a 4% aqueous RuO_4 solution for 2 h.

Scanning Probe Microscopy (SPM). SPM images by tapping mode were obtained at room temperature by a Seiko SPA-400 AFM with a SEIKO SPI-3800N probe station. A rectangle-shaped silicon tip was applied in dynamic force mode (DFM) experiments (spring force contact of 14 N m^{-1} and scan rates of 1 Hz). The thin-film thickness was determined either by SPM by scratching the film and simply scanning the sample surface from center to the edge of spin-coated samples[41] or with a surface profiler (Dektak II A). Consistent results were obtained by using different methods.

Field-Emission Scanning Electron Microscopy (FESEM). PS−PLLA thin-film samples were examined after hydrolysis by FESEM with a JEOL JSM-6700F using accelerating voltages of 1.5 keV. The samples were first sputter-coated with 2−3 nm of platinum.

Results and Discussion

Morphologies of PS—PLLA Thin Films. PS−PLLA thin films were prepared by spin-coating from chlorobenzene (C_6H_5-Cl) solution (1.5 wt % of PS−PLLA) on carbon-coated glass slides. Upon quenching by liquid nitrogen from the melt state at 180 °C, the thermally treated samples were identified by TEM at ambient condition. Because of the staining, the PS microdomains are darker and the PLLA microdomains are lighter.

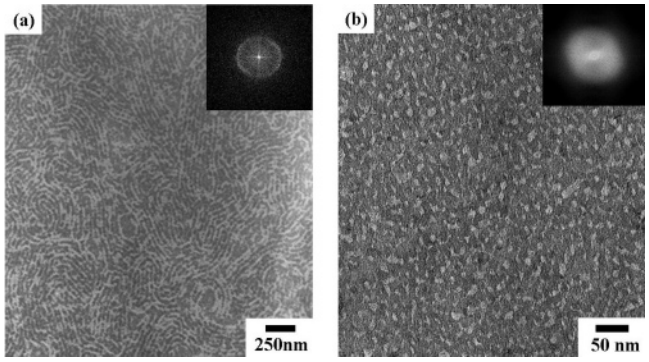

Figure 1. TEM micrographs of (a) S14-L15 ($f_{PS}^{\upsilon} = 0.52$) and (b) S03-L05 ($f_{PS}^{\upsilon} = 0.51$) thin films quenched from 180 °C to 25 °C. In all following figures, the insets show the corresponding Fast Fourier transforms.

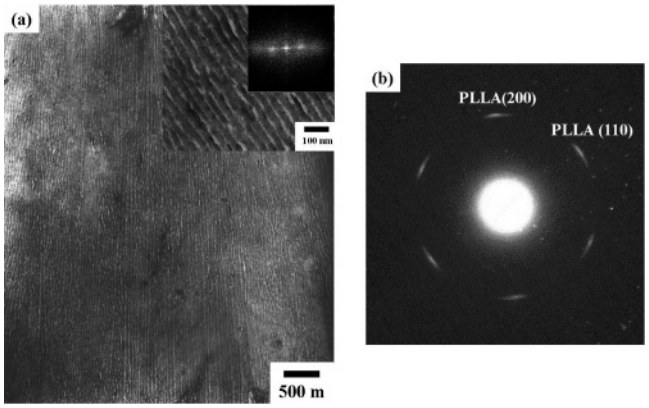

Figure 2. (a) TEM micrograph of oriented S14-L15($f_{PS}^{\upsilon} = 0.52$) microstructure formed on BA; (b) ED pattern obtained from the central area of the micrograph and shown in correct relative orientation.

As expected from the composition, a lamellar microstructure is observed for the quenched high-molecular-weight sample (S14L15 ($f_{PS}^{\upsilon} = 0.52$)) (Figure 1a). The lamellae are randomly distributed so that the fast Fourier transforms (FFTs) show only a ring pattern (inset of Figure 1a). In contrast, a disordered morphology (Figure 1b) is observed for the quenched low-molecular-weight sample (S03L05 ($f_{PS}^{\upsilon} = 0.51$)) which yields a diffuse FFTs pattern (inset of Figure 1b). The formation of disordered morphology indicates significantly lower segregation strength for this low M_n PS−PLLA. Also, both high and low M_n quenched samples are amorphous, as evidenced by electron diffraction experiments. As a result, the disordered morphology of S03L05 is therefore intrinsic textures due to the weak segregation of phase separation, and is not a consequence of PLLA crystallization. Different morphologies (i.e., ordered lamellar and disordered textures) can thus be obtained in strongly segregated high M_n and weakly segregated low M_n PS−PLLA thin films, respectively, in the temperature range studied.

Oriented S14L15 Microstructures from BA. Crystallization of PLLA blocks on the BA crystalline substrate yields large-scale, well-oriented lamellar microstructures. The TEM images of stained samples (Figure 2a) show well-ordered arrays of light, unstained PLLA microdomains alternated with dark, stained PS microdomains. The oriented single-crystal-like oriented lamellar microstructures may be several hundred square micrometers. So, the FFTs pattern exhibits a spotlike first reflection. Figure 2b shows an electron diffraction pattern from the stained thin-film samples. It is an *hk*0 single-crystal diffraction pattern with (200) and (110) spots (PLLA α form with unit cell parameter of $a = 1.07$ nm, $b = 0.595$ nm, $c = 2.78$ nm, and $\alpha = \beta = \gamma = 90°$).[42] As for the PLLA−PCL copolymers,[30] this pattern indicates that the PLLA chain axis is normal to the substrate surface. In addition, PLLA *a* axis is normal to the lamellar microdomains. The crystallographic relationship between the oriented lamellar microdomains and the substrate can be determined by combining this structural information and the examination of thin films by polarized light microscopy. A stripelike texture corresponds to the regions of thicker polymeric material which are formed between elongated crystals of the substrate. The fast growth direction of both substrates is the *b* axis of BA and HMB. The {020} reflections of BA parallel the {200} reflections of crystalline PLLA; the microstructure is indeed oriented along the *b*-axis of BA, suggesting an epitaxial relationship. As for the previous studies on PLLA−PCL (see Figure 6 of ref 30), the (001) PLLA plane and (001) BA plane are in contact, and the *b*-and *a*-axes of PLLA parallel to the *a*- and *b*-axes of BA, respectively. This analysis indicates a lattice matching between PLLA and BA crystals. The structure of BA is known (monoclinic cell with $a = 0.552$ nm, $b = 0.514$ nm, $c = 2.19$ nm, $\alpha = 90°$, $\beta = 97.3°$, and $\gamma = 90°$).[43,44] The dimension of PLLA *a*-axis is nearly double that of BA *b*-axis, and PLLA *b*-axis is nearly equal to that of BA *a*-axis; the corresponding mismatches are 4% and 7%, respectively. The ordering mechanism for strongly segregated PS−PLLA microstructures may therefore involve three driving forces: (1) a lattice matching that generates oriented microstructures through the crystallographic epitaxial matching of the PLLA block and organic substrate, (2) a directional eutectic solidification whereby PS−PLLA is directionally solidified via crystallization of the solvent at the eutectic point, and (3) a crystallization-induced orientation via directional crystallization of PLLA on the substrates. As discussed below, these ordering mechanisms were tested by various experiments.

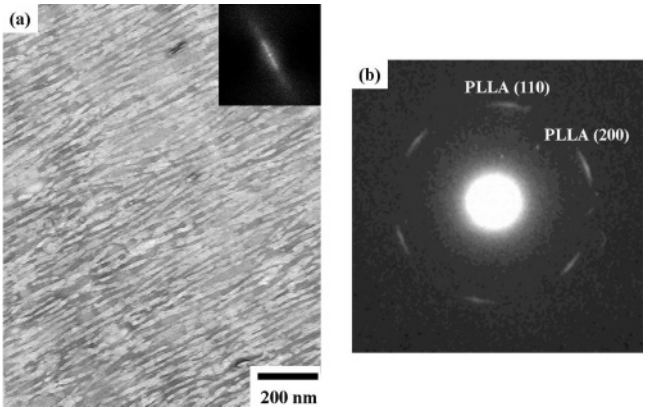

Figure 3. (a) TEM micrograph of oriented S14-L15($f_{PS}^{\upsilon} = 0.52$) microstructure formed on HMB; (b) ED pattern from the central area of the micrograph and shown in correct orientation.

Lattice Matching Effect for Oriented S14L15 Microstructures. Involvement of lattice matching in microstructure orientation was tested by resorting to another substrate, namely HMB. Oriented S14L15 microstructures induced by HMB are obtained over large domains (Figure 3a). The FFTs diffraction pattern (inset of Figure 3a) still displays a spotlike first reflection perpendicular to the *b* axis of HMB crystals, but the reflection is more scattered than for BA, indicating that HMB induces a lower microstructure orientation than BA. The ED pattern (Figure 3b) indicates that the chain axis is perpendicular to the substrate surface. The HMB unit cell parameters are $a = 0.892$ nm, $b = 0.886$ nm, $c = 0.53$ nm, $\alpha = 44.3°$, $\beta = 116.4°$, and $\gamma = 119.3°$.[45] No obvious lattice matching between the ab PLLA plane and the HMB *ab* plane is apparent, although large-scale microstructure orientation has been obtained. Lattice matching

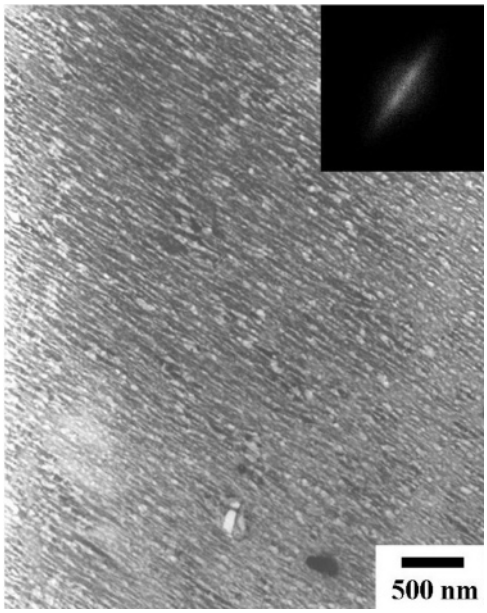

Figure 4. TEM micrograph of S14-L15 ($f_{PS}^{\nu} = 0.52$) thin film after directional eutectic solidification with BA.

can improve the microstructure orientation but is not critical in the ordering mechanism of strongly segregated PS−PLLA block copolymers.

S14L15 Morphology via Directional Eutectic Solidification. To test the directional eutectic solidification effect in strongly segregated PS−PPLA, the S14L15 thin films were quenched while BA was still molten. Crystalline BA powders were spread on a cover slide. The polymer-coated glass slide was placed side down on the BA and melted at 150 °C. After dissolution of the block copolymer in molten BA, the preparation was quenched in liquid nitrogen. No significant crystalline diffraction was observed by SAED. The PS−PLLA thin film dose not crystallizes during the directional eutectic solidification of BA even though the temperatures are below Tm of PLLA. The time scales involved in directional eutectic solidification appear to be much shorter than the time required for nucleation and growth of PLLA crystals. Bright-filed images of the RuO_4-stained films indicate a large-scale orientation of the S14L15 microstructures (Figure 4). Also, a bright streak perpendicular to the BA *b* axis is observed in the FFTs (inset of Figure 4). The interface of the oriented S14L15 microstructure is blurred in the quenching process. Nevertheless, large-scale orientation of S14L15 microstructure is induced by eutectic solidification even in the absence of PLLA crystallization. Similar results are obtained when using HMB, further confirming that directional eutectic solidification alone can induce orientation in strongly segregated PS−PLLA. Park and co-workers have already made similar analysis to explain the orientation of PS−PMMA by BA—note that in this case both blocks are noncrystallizable.[29]

S03L05 Morphology via Directional Eutectic Solidification. Is strong segregation of PS−PLLA copolymers (S14L15) needed in order to induce large-scale microstructure orientation through directional eutectic solidification? As a test, the above procedure by quenching in liquid nitrogen was repeated, but for a weakly segregated, low M_n S03L05 sample. Again, no significant crystalline diffraction was obtained by SAED. Figure 5a shows a bright-field TEM image of the PS−PLLA thin films stained with RuO_4. In contrast to the oriented lamellar microstructures observed in S14L15 thin films (e.g., Figure 4), the S03L05 thin film from BA substrate displays a disordered morphology with randomly distributed dark PS and bright PLLA

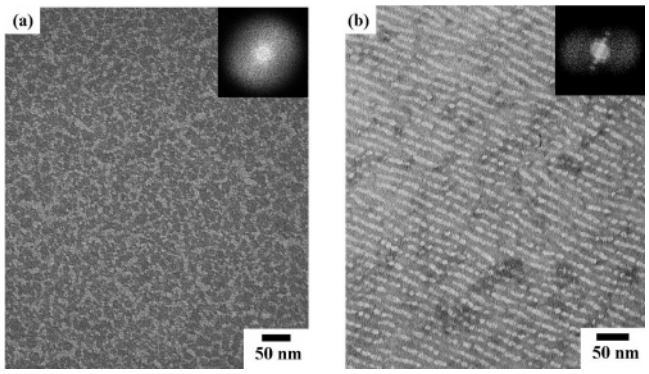

Figure 5. TEM micrographs of S03-L05 ($f_{PS}^{\nu} = 0.51$) thin films (a) solidified from eutectic BA−polymer solution and (b) PLLA directionally crystallized on BA substrate at 80 °C for 30 min.

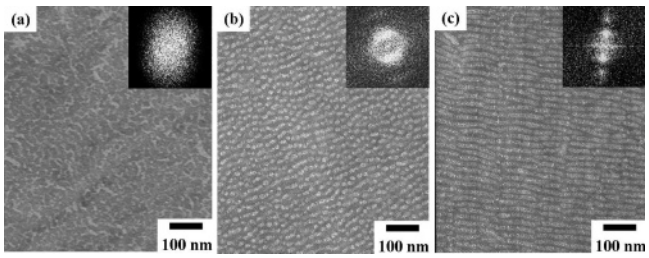

Figure 6. TEM micrographs of S03-L05 ($f_{PS}^{\nu} = 0.51$) thin films (a) solidified from eutectic HMB−polymer solution and (b, c) PLLA directionally crystallized on HMB substrate at 80 °C for (b) 3 min and (c) 30 min.

microdomains, and thus a diffused FFTs pattern (inset of Figure 5a). Again, a comparable morphology is obtained when using HMB (Figure 6a). These morphological observations thus indicate that the segregation strength is critical to induce microstructure orientation of PS−PLLA by directional eutectic solidification.

Crystallization-Induced Oriented S03L05 Microstructures. As just demonstrated, large-scale oriented microstructures of S03L05 cannot be obtained by directional eutectic solidification. What driving force can govern crystallization-induced oriented microstructures in S03L05 system? The spin-coated S03L05 thin-film samples first dissolved in BA at 150 °C, and they were rapidly placed on a hot plate at 80 °C for 30 min. BA crystallized first directionally as large single crystals elongated in the *b* direction. Crystallization of PLLA blocks on the BA substrate took place later, and resulted in large-sized oriented domains of S03L05 (Figure 5b). The microstructure orientation is simply induced by crystallization irrespective of strong or weak segregation strength. An arced pattern is obtained by FFTs (inset of Figure 5b). In contrast to the S14L15 (e.g., Figure 2a), the oriented S03L05 microstructure displays some noncontinuous segments. The origin of this unusual morphology will be discussed below. HMB was also used to induce the oriented crystallization of S03L05 to test the impact of lattice matching. The oriented S03L05 microstructure is similar from HMB (Figure 6c) and BA, and yields similar arced patterns (FFTs, inset of Figure 6c). Apparently, lattice matching does not help improve the crystallization-induced microstructure orientation in S03L05.

The genesis and development of crystallization-induced oriented microstructures on HMB at 80 °C can be followed by quenching the samples after different crystallization times. Initially, a disordered morphology was obtained through directional crystallization of HMB (Figure 6a). After 3 min PLLA crystallization, the S03L05 lamellar microstructures appear and

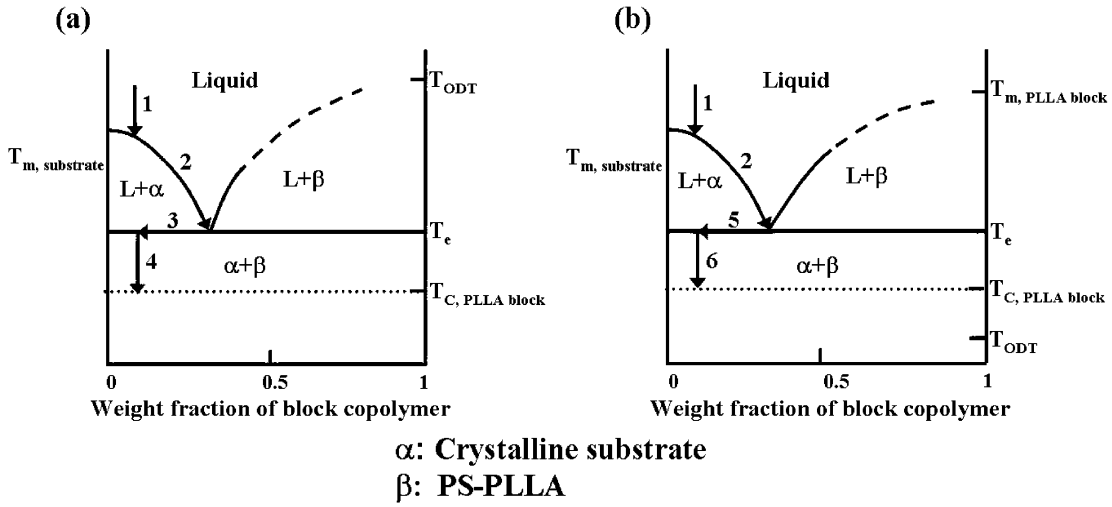

Figure 7. Suggested phase diagrams of crystallizable solvent−polymer systems for (a) strongly segregated high M_n and (b) weakly segregated low M_n PS−PLLA.

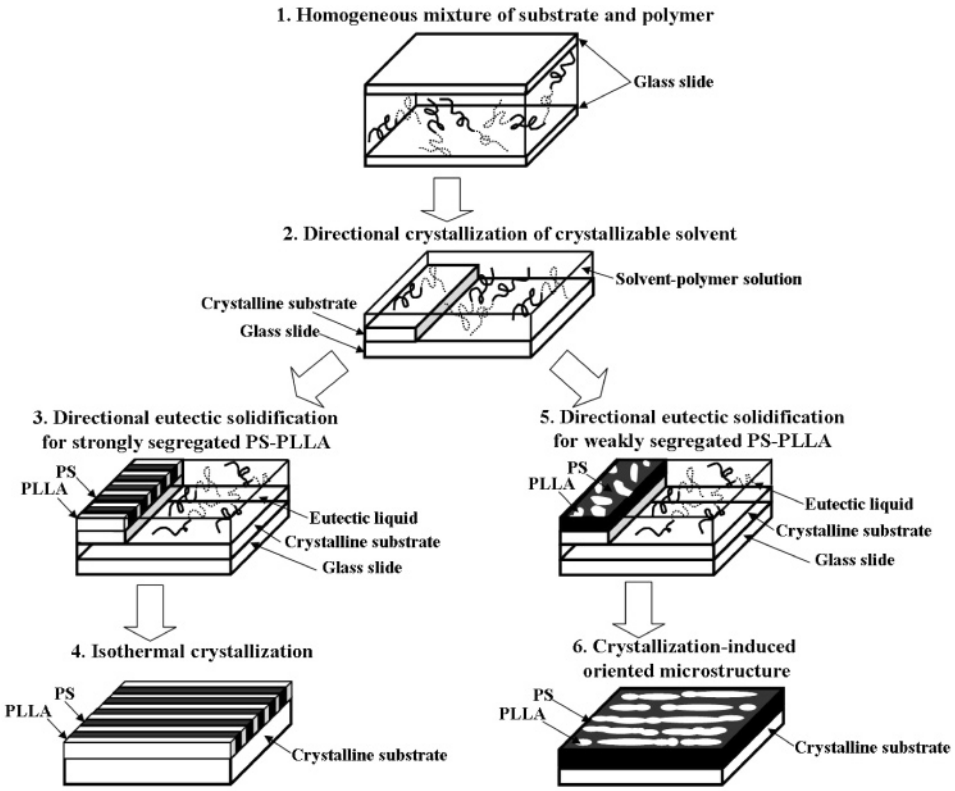

Figure 8. Illustration of morphological evolution for the oriented microstructures in PS−PLLA.

exhibit some orientation even though the microdomains are noncontinuous (Figure 6b). After 30 min, however, the noncontinuous S03L05 microdomains begin to link, and then connect to a significant extent (Figure 6c). The evolution of the FFTs insets in Figure 6. Note that this morphological evolution takes place at 80 °C, below the T_g of bulk PS. It is thus likely that the T_g of PS decreases significantly in the PS−PLLA thin films. This phenomenon was also observed by De Rosa and co-workers.[27] The formation of oriented S03L05 microstructure follows complex scenario. It is induced by nucleation of PLLA taking place randomly in the disordered PLLA domains. With increasing PLLA crystallinity, the individual PLLA microdomains gradually interconnect to form the lamellae. Meanwhile, the PS microdomains are rejected on both sides of the PLLA lamellae, thus creating the alternating PLLA and PS layers. Thus, crystallization-induced oriented S03L05 microstructure results mainly from directional crystallization of PLLA on crystalline substrates, with limited impact of directional eutectic solidification and lattice matching effect.

Origins of Induced Orientation. The induction of oriented microstructures in strongly segregated block copolymers has been clearly analyzed by De Rosa and co-workers in term of the directional eutectic solidification concept.[27] The overall phase transformation has been divided in three stages as shown in a hypothetical solvent−polymer phase diagram (Figure 3 in ref 27). A similar solvent−polymer phase diagram for strongly segregated PS−PLLA thin films (S14L15) is shown in Figure 7a. The corresponding morphological evolution, following the stages 1 → 2 → 3 → 4 of Figure 7a, is indicated in Figure 8. The eutectic point is intrinsically the intersection of melting-point depression liquidus curve of crystallizable solvent with order−disorder temperature depression liquidus (that is the

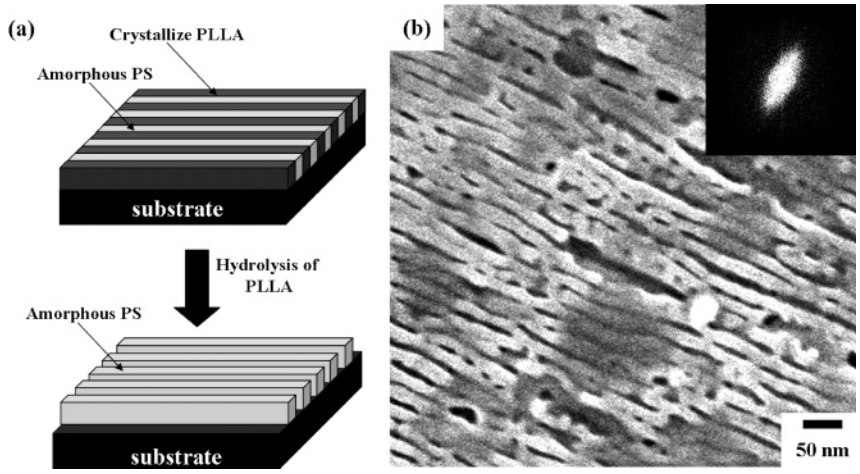

Figure 9. (a) Illustration and (b) FESEM image of oriented S14L15 ($f_{PS}^{\nu} = 0.52$) lamellar thin films induced by a crystallizable solvent after hydrolysis of PLLA.

microphase separation) curve of PS−PLLA. At high temperature, the solvent−polymer solution system is a homogeneous liquid (stage 1). When decreasing the temperature below the melting-point depression liquidus curve, solvent starts to crystallize and forms an oriented crystalline substrate. Upon further decreasing of the temperature, and as growth of the substrate precedes, the polymer concentration in the remaining solution increases (stage 2). When temperature reaches the eutectic temperature, the solution with eutectic composition begins to directionally solidify on the preexisting crystalline substrate. Large-scale lamellar PS−PLLA microstructures are formed (stage 3); the strongly segregated PS−PLLA (S14L15) from directional eutectic solidification shown in Figure 4. After directional eutectic solidification, well-oriented lamellar microstructures with an alternation of flat-on single layers of crystalline PLLA lamellae and of amorphous layers of PS is formed (stage 4). In this scenario, the formation of large-sized, oriented PS−PLLA microstructures results mainly from directional eutectic solidification, with a more limited contribution on lattice matching to improve the orientation order of the microdomains.

For the weakly segregated PS−PLLA thin films (S03L05), the order−disorder transition temperature (T_{ODT}) of PS−PLLA is below the crystallization window of the PLLA component. Therefore, the ordered microstructures are not formed before crystallization of PLLA. The hypothetical phase diagram and the morphological evolution must differ from the strongly segregated PS−PLLA. A modified solvent−polymer phase diagram is thus proposed as shown in Figure 7b, and the corresponding morphological evolution, following the stages 1 → 2 → 5 → 6 of Figure 7b, is indicated in Figure 8. Here, the eutectic point is the intersection of the melting-point depression liquidus curve of crystallizable solvent with liquidus curve of PLLA. At high temperature (stage 1), the solvent−polymer system is liquid. Crystallization of the solvent takes place on cooling below melting-point depression liquidus curve. Upon cooling, depletion of solvent due to crystallization increases the polymer concentration in the remaining solution toward eutectic composition (stage 2). When reaching the eutectic temperature, the eutectic liquid solidifies and transforms into an oriented crystalline substrate; the amorphous PS−PLLA thin film forms a disordered morphology (stage 5). This stage is illustrated in Figures 5a and 6a for BA and HMB solvents, respectively. At this stage, no significant crystallinity is detected by SAED. Because of the nucleation barrier for PLLA crystallization, the PS−PLLA thin film dose not crystallizes during directional eutectic solidification even though the eutectic temperature is below the melting temperature of PLLA. The PLLA crystallization delays and takes place randomly on the solidified disordered microdomains (Figure 6b) while holding temperature at low enough temperature and with enough time to allow PLLA homogeneous nucleation. In this process, the individual PLLA microdomains gradually interconnect to form, ultimately fully develop PLLA lamellae (stage 6) (Figure 5b and Figure 6c for the case of BA and HMB, respectively). Consequently, directional crystallization of PLLA on crystalline substrate is mainly involved in the formation of oriented microstructures for weakly segregated PS−PLLA thin-film system.

Nanopatterned Templates by Hydrolysis. For practical applications, the PLLA component in the oriented microdomains can be selectively degraded by hydrolysis to form trenchlike patterned topographic surfaces. Hillmyer and co-workers[37] dissolved 2g of sodium hydroxide in a 40/60 (by volume) solution of methanol/water at 60 °C to degrade amorphous PLLA. Hydrolysis of well-oriented PS−PLLA thin film is shown in Figure 9a. After hydrolysis of amorphous PLLA, the oriented S14L15 ($f_{PS}^{\nu} = 0.52$) thin-film samples from BA form trenchlike nanochannel arrays, as imaged by FESEM (Figures 9b). By contrast to the FFTs of oriented S14L15 ($f_{PS}^{\nu} = 0.52$) thin-film samples from BA (inset of Figure 2a), the corresponding FFTs diffraction pattern (inset of Figure 9b) displays only a bandlike reflection, less well resolved than for the original, nondegraded sample (inset of Figure 2a). This loss is attributed to the presence of many local defects on the oriented nanochannels, possibly linked with the difficulty to hydrolyze crystalline PLLA portion as opposed to amorphous PLLA. Using harsher hydrolyzing conditions at higher temperature may be required to improve the quality of the nanopattern. This approach is still in progress. Periodic nanochannel thin films are very useful for lithography. After degradation of PLLA, the nanopatterns may be transferred to the substrate by reactive etching.[46,47] Additionally, the patterns can be used for thermal evaporation of a component into the previously removed regions so as to create nanoscale objects from templation.[48] Nevertheless, these preliminary experiments suggest a possible way to prepare large-scale trenchlike microdomains from PS−PLLA diblock copolymer thin films by exploiting the hydrolysis character of the polyester. The formation of such lamellar nanochannels arrays provides a simple path to prepare nanopatterned templates.

Conclusions

A unique morphology of PS−PLLA copolymers with large-sized, well-oriented microstructures was formed from different crystallizable solvents. The orientation mechanisms were studied in details. The directional eutectic solidification induces oriented microstructures in strongly segregated PS−PLLA thin films through the eutectic behavior of microphase separation and directional crystallization of crystallizable solvents. In contrast, oriented microstructures of the weakly segregated PS−PLLA thin films were formed by directional crystallization of PLLA on the crystalline substrate. Moreover, since the PLLA block can be removed by hydrolysis, we present a convenient way to prepare trenchlike nanochannels from PS−PLLA thin films.

Acknowledgment. This research was supported by the National Science Council (NSC) of Taiwan NSC94-2216-1-007-040. We would like to thank Ms. P.-C. Chao and Mr. Y. -F. Lu of Regional Instruments Center at NCHU for their help in TEM and FESEM experiments, respectively.

References and Notes

(1) For a recent review, see: Park, C.; Yoon, J.; Thomas, E. L. *Polymer* **2003**, *44*, 6725.
(2) Kim, G.; Libera, M. *Macromolecules* **1998**, *31*, 2569.
(3) Fukunaga, K.; Elbs, H.; Magerle, R.; Krausch, G. *Macromolecules* **2000**, *33*, 947.
(4) Temple, K.; Kulbaba, K.; Power-Billard, K. N.; Manners, I.; Leach, A.; Xu, T.; Russell, T. P.; Hawker, C. J. *Adv. Mater.* **2003**, *15*, 297.
(5) Kim, S. H.; Misner, M. J.; Xu, T.; Kimura, M.; Russell, T. P. *Adv. Mater.* **2004**, *16*, 226.
(6) Van Dijk, M. A.; Van den Berg, R. *Macromolecules* **1995**, *28*, 6773.
(7) Mansky, P.; Harrison, C. K.; Chaikin, P. M.; Register, R. A.; Yao, N. *Appl. Phys. Lett.* **1996**, *68*, 2586.
(8) Lammertink, R. G. H.; Hempenius, M. A.; Van den Enk, J. E.; Chan, V. Z.-H.; Thomas, E. L.; Vancso, G. J. *Adv. Mater.* **2000**, *12*, 98.
(9) Hahm, J.; Sibener, S. J. *Langmuir* **2000**, *16*, 4766.
(10) Ho, R.-M.; Tseng, W.-H.; Fan, H.-W.; Chiang, Y.-W.; Lin, C.-C.; Huang, B.-H.; Kao, B.-T. *Polymer* **2005**, *46*, 9362.
(11) Keller, A.; Pedemonte, E.; Willmouth, F. M. *Nature (London)* **1970**, *225*, 538.
(12) Albalak, R. J.; Thomas, E. L. *J. Polym. Sci., Part B Polym. Phys.* **1993**, *32*, 37.
(13) Koppi, K. A.; Tirrell, M.; Bates, F. S. *Phys. Rev. Lett.* **1993,** *70*, 1449.
(14) Chen, Z.-R.; Kornfield, J. A.; Smith, S. D.; Grothaus, J. T.; Satkowski, M. M. *Science* **1997**, *277*, 1248.
(15) Albalak, R. J.; Thomas, E. L.; Capel, M. S. *Polymer* **1997**, *38*, 3819.
(16) Morkved, T. L.; Lu, M.; Urbas, A. M.; Ehrichs, E. E.; Jaeger, H. M.; Mansky, P.; Russell, T. P. *Science* **1996**, *273*, 931.
(17) Thurn-Albrecht, T.; Schotter, J.; Kästle, G. A.; Emley, N.; Shibauchi, T.; Krusin-Elbaum, L.; Guarini, K.; Black, C. T.; Tuominen, M. T.; Russell, T. P. *Science* **2000**, *290*, 2126.
(18) Mansky, P.; Liu, Y.; Huang, E.; Russell, T. P.; Hawker, C. *Science* **1997**, *275*, 1458.
(19) Huang, E.; Rockford, L.; Russell, T. P.; Hawker, C. J. *Nature (London)* **1998**, *395*, 757.
(20) Olayo-Valles, R.; Lund, M. S.; Leighton, C.; Hillmyer, M. A. *J. Mater. Chem.* **2004**, 14, 2729.
(21) Rockford, L.; Liu, Y.; Mansky, P.; Russell, T. P. *Phys. Rev. Lett.* **1999**, *82*, 2602.
(22) Heier, J.; Genzer, J.; Kramer, E. J.; Bates, F. S.; Walheim, S.; Krausch, G. *J. Chem. Phys.* **1999**, *111*, 11101.
(23) Kim, S. O.; Solak, H. H.; Stoykovich, M. P.; Ferrier, N. J.; dePablo, J. J.; Nealey, P. F. *Nature*, **2003**, *424*, 411.
(24) Hashimoto, T.; Bodycomb, J.; Funaki, Y.; Kimishima, K. *Macromolecules* **1999**, *32*, 952.
(25) Segalman, R. A.; Yokoyama, H.; Kramer, E. J. *Adv. Mater.* **2001**, *13*, 1152.
(26) Cheng, J. Y.; Ross, C. A.; Thomas, E. L.; Smith, H. I.; Vancso, G. J. *Appl. Phys. Lett.* **2002**, *81*, 3657.
(27) De Rosa, C.; Park, C.; Thomas, E. L.; Lotz, B. *Nature (London)* **2000**, *405*, 433.
(28) De Rosa, C.; Park, C.; Lotz, B.; Wittmann, J. C.; Fetters, L. J.; Thomas, E. L. *Macromolecules* **2000**, *33*, 4871.
(29) Park, C.; De Rosa, C.; Thomas, E. L. *Macromolecules* **2001,** 34, 2602.
(30) Ho, R.-M.; Hsieh, P.-Y.; Tseng, W.-H.; Lin, C.-C.; Huang, B.-H.; Lotz, B. *Macromolecules* 2**003**, *36*, 9085.
(31) Park, C.; De Rosa, C.; Lotz, B.; Fetters, L. J.; Thomas, E. L. *Macromol. Chem. Phys.* **2003**, *204*, 1514.
(32) Ho, R.-M.; Lin, F.-H.; Tsai, C.-C.; Lin, C.-C.; Ko, B.-T.; Hsiao, B. S.; Igors, S. *Macromolecules* **2004**, *37*, 5985.
(33) Wittmann, J. C.; Lotz, B. *J. Polym. Sci., Polym. Phys. Ed.* **1981**, 1837.
(34) Wittmann, J. C.; Lotz, B. J. Polym. Sci. *Polym. Phys. Ed.* **1981**, 1853.
(35) Wittmann, J. C.; Hodge, A. M.; Lotz, B. *J. Polym. Sci., Polym. Phys. Ed.* **1983**, 2495.
(36) Tsuji, H.; Ikada, Y. J. *Polym. Sci., Part A: Polym. Chem.* **1998**, *36*, 59.
(37) Zalusky, A. S.; Olayo-Valles, R.; Taylor, C. J.; Hillmyer, M. A. *J. Am. Chem. Soc.* **2001**, *123*, 1519.
(38) Leiston-Belanger, J. M.; Russell, T. P.; Drockenmuller, E.; Hawker, C. J. *Macromolecules* 2**005**, *38*, 7676.
(39) Ko, B.-T.; Lin, C.-C. *J. Am. Chem. Soc.* **2001**, *123*, 7973.
(40) Ho, R.-M.; Chiang, Y.-W.; Tsai, C.-C.; Lin, C.-C.; Ko, B.-T.; Huang, B.-H. *J. Am. Chem. Soc.* **2004**, *126*, 2704.
(41) Spatz, J. P.; Sheiko, S.; Möller, M. *Adv. Mater.* **1996**, *8*, 513.
(42) Cartier, L.; Okihara, T.; Ikada, Y.; Tsuji, H.; Puiggali, J.; Lotz, B. *Polymer* **2000**, 41, 8909.
(43) Sarma, K. R.; Shlichta, P. J.; Wilcox, W. R.; Lefever, R. A. *J. Cryst. Growth* **1997**, 174, 487.
(44) Holmbäck, X.; Rasmuson, A. C. *J. Cryst. Growth* **1999**, *199*, 780.
(45) Brockway, L. O.; Robertson, J. M. *J. Chem. Soc.* **1939**, 1324.
(46) Lammertink, R. G.; Hempenius, M. G.; Van den Enk, J. E.; Chan, V. Z.-H.; Thomas, E. L.; Vancso, G. J. *Adv. Mater.* **2000**, *12*, 98.
(47) Park, M.; Harrison, C. K.; Chaikin, P. M.; Register, R. A.; Adamson, D. H. *Science* **1997**, *276*, 1401.
(48) Li, R. R.; Dapkus, P. D.; Thompson, M. E.; Jeong, W. G.; Harrison, C.; Chaikin, P. M.; Register, R. A.; Adamson, D. H. *Appl. Phys. Lett.* **2000**, *76*, 1689.

MA0608929